Structure-Guided Design of Substituted Biphenyl Butanoic Acid Derivatives as Neprilysin Inhibitors

Toshio Kawanami,[||] Rajeshri G. Karki,*,[||] Emma Cody, Qian Liu, Guiqing Liang, Gary M. Ksander, Dean F. Rigel, Nikolaus Schiering, Yongjin Gong, Gary M. Coppola, Yuki Iwaki, Robert Sun, Alan Neubert, Li Fan, Sara Ingles, Allan D'Arcy, Frederic Villard, Paul Ramage, Arco Y. Jeng, Jennifer Leung-Chu, Jing Liu, Michael Beil, Fumin Fu, Wei Chen, Frederic Cumin, Christian Wiesmann, and Muneto Mogi*

ACCESS | Metrics & More | Article Recommendations | Supporting Information

ABSTRACT: Inhibition of neprilysin (NEP) is widely studied as a therapeutic target for the treatment of hypertension, heart failure, and kidney disease. Sacubitril/valsartan (LCZ696) is a drug approved to reduce the risk of cardiovascular death in heart failure patients with reduced ejection fraction. LBQ657 is the active metabolite of sacubitril and an inhibitor of NEP. Previously, we have reported the crystal structure of NEP bound with LBQ657, whereby we noted the presence of a subsite in S1′ that has not been explored before. We were also intrigued by the zinc coordination made by one of the carboxylic acids of LBQ657, leading us to explore alternative linkers to efficiently engage zinc for NEP inhibition. Structure-guided design culminated in the synthesis of selective, orally bioavailable, and subnanomolar inhibitors of NEP. A 17-fold boost in biochemical potency was observed upon addition of a chlorine atom that occupied the newly found subsite in S1′. We report herein the discovery and preclinical profiling of compound **13**, which paved the path to our clinical candidate.

KEYWORDS: Neprilysin, crystal structure, structure-based design, structure−activity relationship
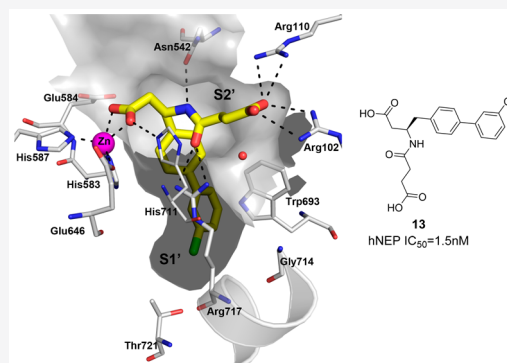
NEP (EC 3.4.24.11; neprilysin, neutral endopeptidase, enkephalinase; atriopeptidase) is a zinc-dependent type II integral membrane endopeptidase belonging to the peptidase M13 family. It cleaves a variety of peptide substrates such as atrial natriuretic peptide (ANP, also known as ANF), brain natriuretic peptide (BNP), bradykinin, adrenomedullin, and endothelin-1.[1] The increase in circulating ANP levels achieved by NEP inhibition has favorable implications for the treatment of congestive heart failure and chronic renal failure.[2,3] Sacubitril/valsartan (LCZ696) is a drug approved to reduce the risk of cardiovascular death and hospitalization for patients with chronic heart failure (NYHA Class II−IV) and reduced ejection fraction (HFrEF).[4] LCZ696 (Figure 1) is a sodium salt complex containing the anionic forms of the angiotensin II type 1 receptor antagonist valsartan and the NEP inhibitor prodrug sacubitril.[5] Upon oral administration, LCZ696 provides rapid systemic exposure to sacubitril and valsartan. Sacubitril is converted by enzymatic cleavage of the ethyl ester to the active metabolite LBQ657 (compound **1**, Figure 2b).[6]

We have reported the crystal structure of LBQ657 in complex with NEP, rationalizing its potency and selectivity.[7]
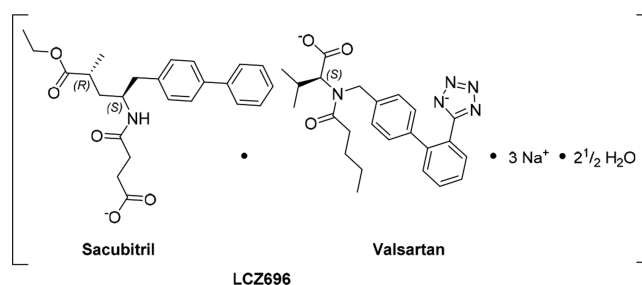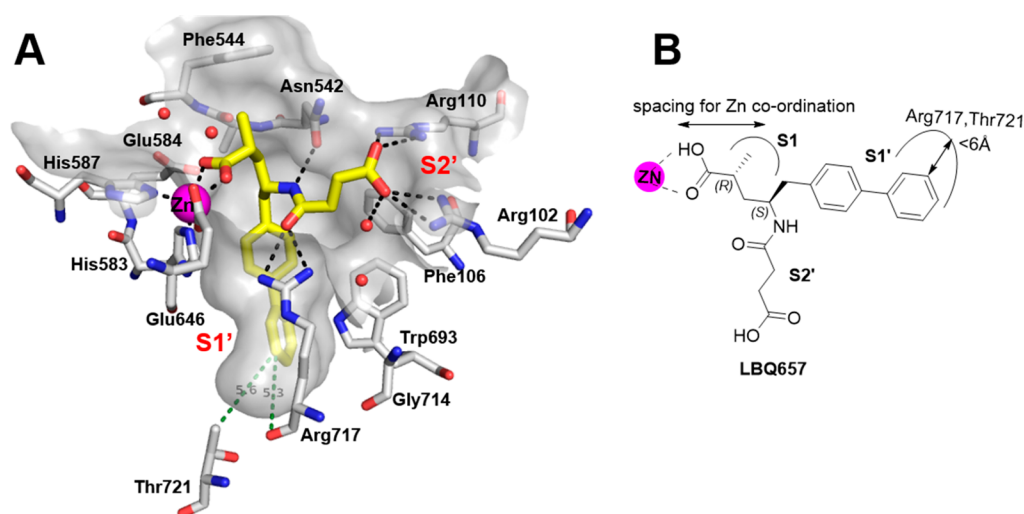

Figure 1. Schematic structural formula of LCZ696, showing sacubitril and valsartan, in their respective anionic forms.

LBQ657 binds in the active site of NEP making an intricate network of H-bonding and van der Waals interactions that

Figure 2. (a) Crystal structure of NEP (white carbon atoms) with LBQ657 (yellow) showcasing the S1′ subsite. The ligand binding pocket is shown in gray and zinc atom is in magenta. H-bonding interactions are shown as black dotted lines and crystallographic waters are shown as red spheres. The distance between the meta position of the aromatic ring and two S1′ residues (Arg717 and Thr721) is shown in green. (b) Schematic representation of the concepts studied in this paper.

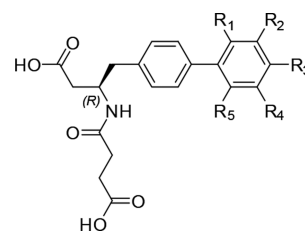**Table 1. Impact of Linker Length on NEP Inhibitory Activity**[a]
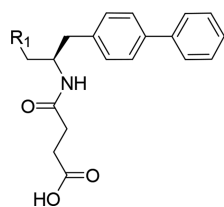
Compound	R_1	hNEP IC_{50} (nM)
1 (LBQ657)	$CH(CH_3)COOH$ (R)	6
2	CH_2COOH	550
3	$C(CH_3)_2COOH$	20
4	COOH	25

[a]IC_{50} values are the mean of at least two independent assays.
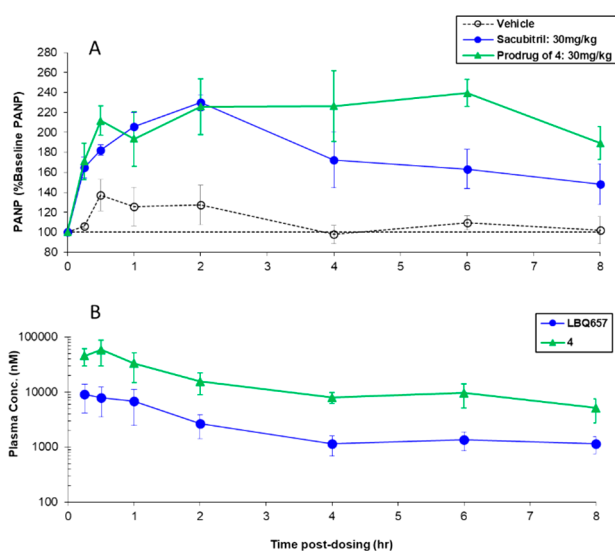
Figure 3. (a) Pharmacodynamic and (b) pharmacokinetic time courses of orally administered prodrug of **4** at 30 mg/kg in the ANP potentiation model in conscious rats.
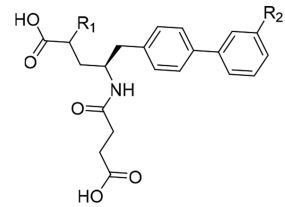
Table 2. SAR of S1′ Substitution[a]

| Compound	R_1	R_2	R_3	R_4	R_5	hNEP IC_{50} (nM)
4	H	H	H	H	H	25
5	Cl					8
6	F					24
7	CH_3					21.3
8	CN					792
9	OCH_3					4.5
10	OC_2H_5					413
11	CF_3					1370
12	OCF_3					212
13		Cl				1.5
14		F				6.7
15		NH_2				44
16		CH_3				1.6
17		C_2H_5				5.4
18		OCH_3				60
19		CF_3				111
20		OCF_3				275
21		CN				6.9
22		NO_2				26
23		$NHCOCH_3$				4862
24			Cl			1950
25			F			1500
26		Cl			OCH_3	0.38
27	OCH_3	Cl				4182
28		Cl		F		54

[a]IC_{50} values are the mean of at least two independent assays.

involves all functional groups of the compound giving rise to the high inhibitory potency of 5 nM[8] (Figure 2a).

Table 3. Testing SAR of S1′ Substitution in Pentanoic Acid Series[a]

Compound	R_1	R_2	hNEP IC_{50} (nM)
LBQ657	(R)-CH$_3$	H	6
29	(S)-CH$_3$	Cl	2
30	(R)-CH$_3$	Cl	0.3
31	rac-CH$_3$	Cl	0.8

[a]IC_{50} values are the mean of at least two independent assays.

Scheme 1. Typical Synthetic Route Utilized for Biphenylbutanoic Acid Derivatives[a]
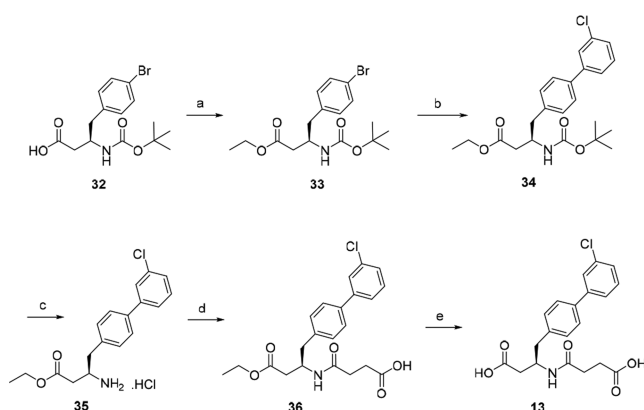
[a]Reagents and conditions: (a) EtI, NaHCO$_3$, DMF, rt; (b) 3-Cl-C$_6$H$_4$-B(OH)$_2$, Pd(PPh$_3$)$_4$, aq. Na$_2$CO$_3$, DME, 95 °C; (c) 4 M HCl in 1,4-dioxane; (d) succinic anhydride, DIPEA, DCM; (e) 1 M aq. NaOH, THF, MeOH, rt; 1 M aq. HCl.

In the crystal structure of LBQ657 in complex with NEP we observed a small subsite in S1′ extending out from the meta-position of the phenyl ring toward the backbone carbonyl atom of Arg717 and side chain of Thr721 (Figure 2). To the best of our knowledge, interactions in this region were not explored at the time when we conducted the study, leading us to probe the structure–activity relationship (SAR) at this position. One other observation made from the cocrystal structure was the zinc coordination made by LBQ657. Unlike many previously reported NEP inhibitor complex structures,[9−13] LBQ657 has a longer linker between the zinc coordinating group (carboxylate) and the chiral carbon atom that anchors the S1′ and S2′ binding moieties (Figure 2b). This led us to study alternative linkers to efficiently engage zinc for NEP inhibition. We investigated both of these findings by initially synthesizing a few rationally designed compounds. Encouraged by the results, we delved into a systematic exploration of the S1′ SAR. In this report we describe the medicinal chemistry optimization, SAR, validation of the binding mode by cocrystallization with NEP, and results from preclinical investigation of selected compounds.

As mentioned above, in four out of the seven previously reported NEP inhibitor cocrystal structures,[10−13] the zinc coordinating moiety, which is either a thiol or phosphonic acid

analog, is separated from the chiral anchor atom by a single linker atom which is either carbon or nitrogen. In LBQ657 there are two atoms including a chiral carbon atom that serves as the linker presenting the carboxylic acid for zinc coordination. We were curious to study the impact of modifying the linker group and hence made compounds 2–4, Table 1. A biochemical assay was developed to assess NEP inhibition *in vitro* using recombinant human NEP (Supporting Information). As shown in Table 1, removing the chiral methyl group in LBQ657 resulted in almost a 100-fold loss in NEP inhibitory activity (compound **2**) while the dimethyl analog **3** was 3-fold less active. Based on these observations one may conclude that the chiral methyl group in LBQ657 rigidifies the linker and facilitates zinc coordination via the carboxylic acid. Shortening the linker length by one carbon atom (**4**) was equipotent to **3** indicating zinc coordination is plausible albeit less efficient. Considering the biochemical potency of **4** was within 5-fold of LBQ657, we characterized the *in vitro* absorption, distribution, metabolism, and elimination (ADME) parameters followed by *in vivo* rat pharmacokinetic (PK) profile. Compound **4** was stable in both rat and human liver microsomes (Clint < 3.42 μL/min/mg in rat and human) and hepatocytes (Clint = 2.1 and 0.68 μL/min per million cells in rat and human, respectively). When administered to Sprague–Dawley rats at 1 mg/kg IV, the plasma clearance of **4** was low (11 mL/min/kg) with a small volume of distribution (0.2 L/kg) and half-life of 2.5 h. Based on our experience with sacubitril the prodrug of LBQ657, the ethyl ester prodrug of **4** was administered orally at 3 mg/kg. The prodrug of **4** showed rapid absorption and complete hydrolysis to generate **4** with a bioavailability of ∼66%.

Encouraged by the PK data, we decided to study the *in vivo* pharmacodynamics (PD) in an ANP potentiation model in conscious rats.[6] In this animal model, conscious chronically cannulated adult male Sprague–Dawley rats were infused intravenously with rat ANP to saturate the natriuretic peptide clearance receptors and, thereby, shift the elimination of ANP to predominantly enzymatic degradation by NEP. Blood samples were withdrawn before dosing with compound or vehicle (baseline) and at various times up to 8 h postdosing to simultaneously assess PK/PD. PD readout was the potentiation (% baseline) of plasma ANP (PANP), which was used as an index of a surrogate for the extent and duration of NEP inhibition. When administered orally at 30 mg/kg, the ethyl ester prodrug of **4** rapidly (within 15 min) augmented PANP (Figure 3a). PANP levels remained elevated for almost the entire experiment, reflecting the compound's long duration of action. Plasma levels of **4** remained >2 μM (Figure 3b). In this model, the prodrug of **4** was found to be more effective than sacubitril when administered at 30 mg/kg orally.

Synthesis of **4** with one less chiral center was much simpler relative to LBQ657. The promising *in vivo* profile of **4** and its simplified synthesis resulted in the selection of **4** as a lead compound for SAR exploration of the S1′ binding moiety. In the LBQ657-bound NEP crystal structure, the distance between the meta position of the second phenyl ring (Figure 2) and the Arg717 backbone carbonyl was 5.3 Å. The side chain of Thr721 was at a distance of ∼5.6 Å. We started out by adding small substituents in this meta position (Table 2) to fill this space.

Compound **13** with chlorine at R2 was 17-times more active than its unsubstituted analog **4**. Methyl analog **16** was equipotent to **13**. The added substituents likely fill the S1′
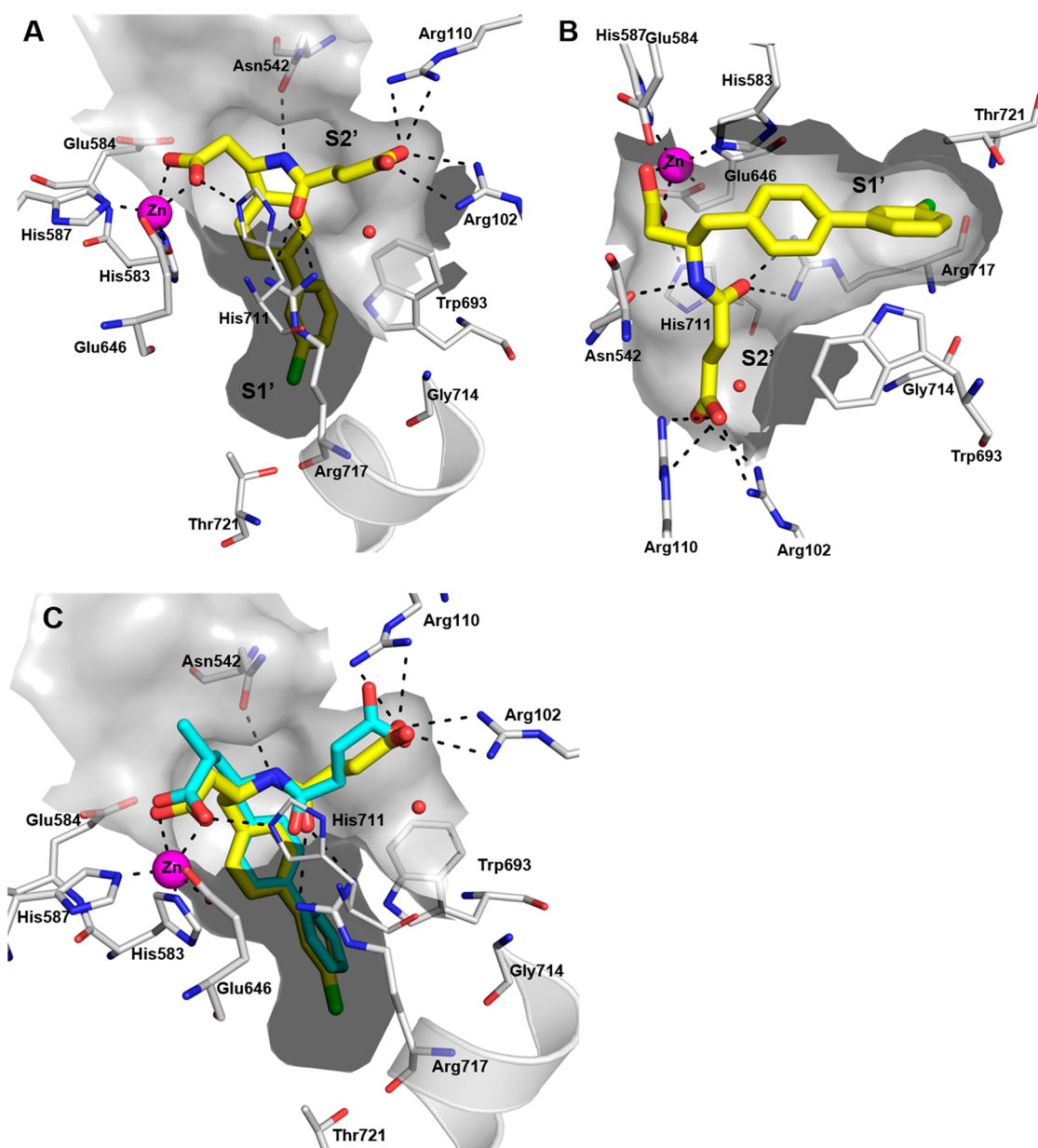
Figure 4. Crystal structure of NEP complexed with **13** (yellow). Zinc atom is shown in magenta. H-bonding interactions are shown as black dotted lines. Chlorine is colored green. (a and b) Two different orientations of the binding site are shown to provide clarity of the interactions. (c) Overlay of crystal structure of LBQ657 (cyan) on **13**.

Table 4. Pharmacokinetic Parameters of 13 and 26 in Sprague Dawley Rat Dosed at 1 mg/kg IV (Parent Compound) and 3 mg/kg PO (Ethyl Ester Prodrug)[a]

Administered Compound	Route	oral C_{max} (nM)	$AUC_{(0-7)}$ (nM·Hours)	CL (mL/min/kg)	Vd_{ss} (L/kg)	Elimination $t_{1/2}$ (IV) (Hours)	%F
13 (active)	IV		8730	5	0.1	0.8	
36 (prodrug)	PO	12600	10100				42
26 (active)	IV		8100	5	0.1	1.0	
39 (prodrug)	PO	5380	5630				25

[a]**36** is the ethyl ester prodrug of **13**; **39** is the ethyl ester prodrug of **26**.

subsite making van der Waals interaction with NEP residues thereby improving the binding affinity. The tolerance for bulk, H-bond donor/acceptor groups was also explored with various R2 substituents (**13**−**23**, Table 2) although no further improvement in potency was observed relative to **13** and **16**. For additional confirmation that the improved potency seen in **13** was indeed a result of filling the space rather than adding a

bulky group, chloro and fluoro substituents were added at ortho (**5** and **6**) and para position of the biphenyl ring (**24** and **25**), respectively. It was interesting to note that adding chlorine at the ortho position was 3-fold better compared to parent compound **4** while being ∼80-fold less active when substituted at the para position (**24**). This led us to further probe the ortho position although being conscious that bigger
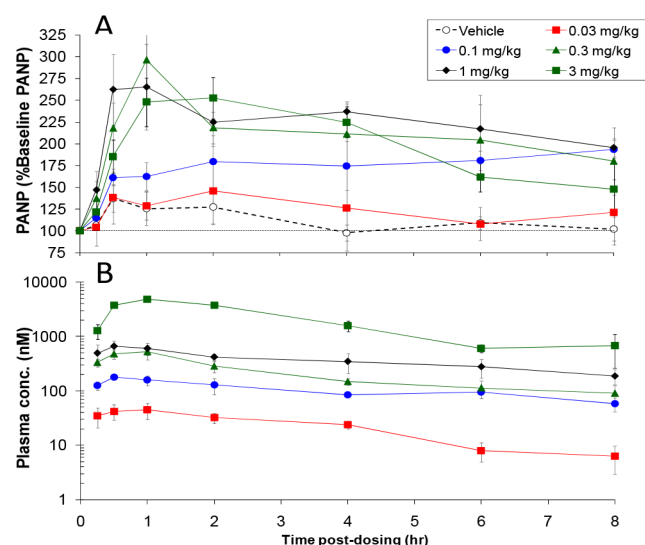
Figure 5. Dose-dependent potentiation of PANP (a) pharmacodynamics and (b) pharmacokinetic time courses of orally administered **36** (ethyl ester prodrug of **13**) in the ANP potentiation model in conscious rats.

substituents would change the torsion between the two phenyl rings of the S1′ biphenyl group. Clearly, with the exception of compound **9** (vs **18**), all substituents at the ortho position (**5–12**) and para position (**24–25**) were less active than the corresponding analogs at the meta position.

Considering the symmetrical nature of the phenyl ring, it was critical to understand the exact location of the methoxy group, so compounds **26** and **27** were synthesized. The significant loss of potency of **27** vs the synergistic improvement seen for **26** led us to conclude that the binding mode of **13** and **26** was comparable to LBQ657. Dimeta substitution was less explored as the initial data with **28** negated the beneficial effect of chloro substitution.

The profound impact on potency improvement upon chloro substitution was investigated on LBQ657. It was astounding to see a perfect translation of the SAR wherein a 20-fold improvement was seen for **30** (Table 3). The *S*-methyl isomer of **30** (compound **29**) and the racemic analog **31** also had improved inhibitory potency relative to LBQ657.

A typical synthesis of biphenylbutanoic acids is depicted in Scheme 1. Treatment of acid **32** with iodoethane in the presence of $NaHCO_3$ afforded ethyl ester **33**, which was then converted to **34** by performing Suzuki–Miyaura coupling. Deprotection of Boc of **34** by HCl/dioxane gave the amine hydrochloride **35**. The amine was reacted with succinic anhydride to afford the amide **36** followed by hydrolysis of the ethyl ester under basic conditions to furnish diacid **13**.

While most synthesized compounds were modeled in the crystal structure of NEP prior to synthesis, we sought to validate the binding mode experimentally. The crystal structure of NEP complexed with **13** was solved using experimental conditions described for LBQ657.[7] The complex of **13** with NEP crystallized in the orthorhombic space group P212121 with two copies in the asymmetric unit diffracting to 2.54 Å resolution.

The structure was solved by molecular replacement. The overall binding mode of **13** is comparable to LBQ657 (Figure 4c) and validates our hypothesis of maintaining the zinc coordination with a shorter linker. The orientation of the

carboxylic acid making zinc coordination is stabilized by interaction with His711 (Figure 4a and 4b). While we noted small movement in side chains of Phe106 and Asn542 relative to LBQ657 X-ray, this did not impact the H-bonding interaction of **13** with Asn542, Arg102, and Arg110. The succinic acid in S2′ has undergone a rotation of 75° relative to LBQ657. Owing to the flexible nature of the succinic acid, alternate orientations cannot be ruled out in solution. The amide carbonyl of **13** makes H-bonding interactions with the side chain of Arg717. In being consistent with our rationale, it was comforting to see the chloro group occupying the S1′ subsite pointing toward the backbone carbonyl of Arg717 and Thr721. It efficiently fills the available space surrounded by side chain from Met579, Asp650, Phe689, Arg717, and Ile718.

We routinely profiled compounds in *in vitro* ADME assays, which gated compound selection for *in vivo* PK/PD studies in rat. The combination of *in vitro* potency and ADME profile resulted in selection of **13** and **26** for PK studies in rats. Oral administration of the ethyl ester prodrug of **13** and **26** showed rapid absorption and hydrolysis to **13** and **26** with bioavailability of 42% and 25%, respectively (Table 4). Both compounds showed low clearance (5 mL/min/kg) and similar apparent half-life after a single IV administration in rats. Considering **13** had ∼2-fold higher bioavailability than **26**, we selected **13** for further *in vivo* profiling studies. Plasma clearance was low for **13** in monkey (3 mL/min/kg) and moderate in dog (29 mL/min/kg). The apparent half-life was 0.8 h for **13** in dog and ∼4 h in monkey.

36, the prodrug of **13**, was rapidly absorbed in all species after a single oral dose. However, the extent of absorbed prodrug converted to active drug was different among rat (99%), dog (5%), and monkey (69%).

The ethyl ester prodrug of **13** was tested in the rat ANP potentiation model. The prodrug (**36**) dose-dependently elevated PANP (Figure 5a). At the highest doses, PANP levels remained elevated for the entire experiment, reflecting the compound's long duration of action. Plasma levels of **13** followed a similar profile (Figure 5b). Upon evaluation across an internal panel of ∼110 enzymes, receptors and ion channels **13** furnished IC_{50} values of >30 μM.

In conclusion, a structure-guided approach resulted in the identification of subnanomolar inhibitors of NEP. We took advantage of the simplified synthesis of the biphenyl butanoic acid series to quickly explore the SAR in the S1′ subsite. The potency drop with a less optimal linker (**4**) was compensated by addition of chlorine in the S1′ subsite. In our preclinical pharmacology model, **13** was found to be 100-fold more potent than sacubitril. While we profiled **13** as a potential clinical candidate, the early success encouraged us to explore other linkers and modifications of the S2′ binding moiety. Results from the new chemical series that evolved from the effort will be published in the future.

■ ASSOCIATED CONTENT

ⓢ Supporting Information

The Supporting Information is available free of charge at https://pubs.acs.org/doi/10.1021/acsmedchemlett.9b00578.

    Synthetic procedures, compound characterization, biochemical and pharmacokinetic study protocol, and crystallographic structure determination of NEP in complex with compound **13** (PDF)

■ AUTHOR INFORMATION

Corresponding Authors

Rajeshri G. Karki − Novartis Institutes for BioMedical Research, Cambridge, Massachusetts 02139, United States; ⦿ orcid.org/0000-0003-2210-5789; Email: rajeshri.karki@novartis.com

Muneto Mogi − Novartis Institutes for BioMedical Research, Cambridge, Massachusetts 02139, United States; Email: muneto.mogi@novartis.com

Authors

Toshio Kawanami − Novartis Institutes for BioMedical Research, Cambridge, Massachusetts 02139, United States

Emma Cody − Novartis Institutes for BioMedical Research, Cambridge, Massachusetts 02139, United States

Qian Liu − Novartis Institutes for BioMedical Research, Cambridge, Massachusetts 02139, United States

Guiqing Liang − Novartis Institutes for BioMedical Research, Cambridge, Massachusetts 02139, United States

†**Gary M. Ksander** − Novartis Institutes for BioMedical Research, Cambridge, Massachusetts 02139, United States

Dean F. Rigel − Novartis Pharmaceuticals Corporation, East Hanover, New Jersey 07936-1080, United States

Nikolaus Schiering − Novartis Institutes for BioMedical Research, CH-4056 Basel, Switzerland

Yongjin Gong − Novartis Institutes for BioMedical Research, Cambridge, Massachusetts 02139, United States

Gary M. Coppola − Novartis Institutes for BioMedical Research, Cambridge, Massachusetts 02139, United States

Yuki Iwaki − Novartis Institutes for BioMedical Research, Cambridge, Massachusetts 02139, United States

Robert Sun − Novartis Institutes for BioMedical Research, Cambridge, Massachusetts 02139, United States

Alan Neubert − Novartis Institutes for BioMedical Research, Cambridge, Massachusetts 02139, United States

Li Fan − Novartis Institutes for BioMedical Research, Cambridge, Massachusetts 02139, United States

Sara Ingles − Novartis Institutes for BioMedical Research, CH-4056 Basel, Switzerland

Allan D'Arcy − Novartis Institutes for BioMedical Research, CH-4056 Basel, Switzerland

Frederic Villard − Novartis Institutes for BioMedical Research, CH-4056 Basel, Switzerland

Paul Ramage − Novartis Institutes for BioMedical Research, CH-4056 Basel, Switzerland

Arco Y. Jeng − Novartis Pharmaceuticals Corporation, East Hanover, New Jersey 07936-1080, United States

Jennifer Leung-Chu − Novartis Pharmaceuticals Corporation, East Hanover, New Jersey 07936-1080, United States

Jing Liu − Novartis Pharmaceuticals Corporation, East Hanover, New Jersey 07936-1080, United States

Michael Beil − Novartis Pharmaceuticals Corporation, East Hanover, New Jersey 07936-1080, United States

Fumin Fu − Novartis Pharmaceuticals Corporation, East Hanover, New Jersey 07936-1080, United States

Wei Chen − Novartis Pharmaceuticals Corporation, East Hanover, New Jersey 07936-1080, United States

Frederic Cumin − Novartis Institutes for BioMedical Research, CH-4056 Basel, Switzerland

Christian Wiesmann − Novartis Institutes for BioMedical Research, CH-4056 Basel, Switzerland

Complete contact information is available at:
https://pubs.acs.org/10.1021/acsmedchemlett.9b00578

Author Contributions

The manuscript was written through contributions of all authors. All authors have given approval to the final version of the manuscript.

Author Contributions

∥T.K. and R.G.K. contributed equally.

Notes

The authors declare no competing financial interest.
†Deceased.

■ ACKNOWLEDGMENTS

■ ABBREVIATIONS

NEP, neprilysin; ANP, atrial natriuretic peptide; BNP, brain natriuretic peptide; HFrEF, heart failure with reduced ejection fraction; ARB, angiotensin II type-1 receptor antagonist; SAR, structure activity relationship

■ REFERENCES

(1) Roques, B. P.; Noble, F.; Daugé, V.; Fournié Zaluski, M. C.; Beaumont, A. Neutral Endopeptidase-24.11 - Structure, Inhibition, and Experimental and Clinical-Pharmacology. *Pharmacol. Rev.* **1993**, 45, 87−146.

(2) Brunner-La Rocca, H. P.; Kiowski, W.; Ramsay, D.; Sütsch, G. Therapeutic benefits of increasing natriuretic peptide levels. *Cardiovasc. Res.* **2001**, 51, 510−520.

(3) Swainson, C. P.; Craig, K. C. Effects of Atrial-Natriuretic-Peptide (99−126) in Chronic Renal-Disease in Man. *Nephrol., Dial., Transplant.* **1991**, 6, 336−341.

(4) McMurray, J. J. V.; Packer, M.; Desai, A. S.; Gong, J. J.; Lefkowitz, M. P.; Rizkala, A. R.; Rouleau, J. L.; Shi, V. C.; Solomon, S. D.; Swedberg, K.; Zile, M. R. Angiotensin-Neprilysin Inhibition versus Enalapril in Heart Failure. *N. Engl. J. Med.* **2014**, 371, 993−1004.

(5) Feng, L.; Karpinski, P. H.; Sutton, P.; Liu, Y.; Hook, D. F.; Hu, B.; Blacklock, T. J.; Fanwick, P. E.; Prashad, M.; Godtfredsen, S.; Ziltener, C. LCZ696: a dual-acting sodium supramolecular complex. *Tetrahedron Lett.* **2012**, 53, 275−276.

(6) Gu, J.; Noe, A.; Chandra, P.; Al-Fayoumi, S.; Ligueros-Saylan, M.; Sarangapani, R.; Maahs, S.; Ksander, G.; Rigel, D. F.; Jeng, A. Y.; Lin, T.-H.; Zheng, W.; Dole, W. P. Pharmacokinetics and Pharmacodynamics of LCZ696, a Novel Dual-Acting Angiotensin Receptor-Neprilysin Inhibitor (ARNi). *J. Clin. Pharmacol.* **2010**, 50, 401−414.

(7) Schiering, N.; D'Arcy, A.; Villard, F.; Ramage, P.; Logel, C.; Cumin, F.; Ksander, G. M.; Wiesmann, C.; Karki, R. G.; Mogi, M. Structure of neprilysin in complex with the active metabolite of sacubitril. *Sci. Rep.* **2016**, 6, 27909.

(8) Ksander, G. M.; Ghai, R. D.; deJesus, R.; Diefenbacher, C. G.; Yuan, A.; Berry, C.; Sakane, Y.; Trapani, A. Dicarboxylic-Acid Dipeptide Neutral Endopeptidase Inhibitors. *J. Med. Chem.* **1995**, *38*, 1689−1700.

(9) Oefner, C.; Roques, B. P.; Fournie-Zaluski, M. C.; Dale, G. E. Structural analysis of neprilysin with various specific and potent inhibitors. *Acta Crystallogr., Sect. D: Biol. Crystallogr.* **2004**, *60*, 392−396.

(10) Oefner, C.; Pierau, S.; Schulz, H.; Dale, G. E. Structural studies of a bifunctional inhibitor of neprilysin and DPP-IV. *Acta Crystallogr., Sect. D: Biol. Crystallogr.* **2007**, *63*, 975−981.

(11) Oefner, C.; D'Arcy, A.; Hennig, M.; Winkler, F. K.; Dale, G. E. Structure of human neutral endopeptidase (neprilysin) complexed with phosphoramidon. *J. Mol. Biol.* **2000**, *296*, 341−349.

(12) Sahli, S.; Frank, B.; Schweizer, W. B.; Diederich, F.; Blum-Kaelin, D.; Aebi, J. D.; Bohm, H. J. Second-generation inhibitors for the metalloprotease neprilysin based on bicyclic heteroaromatic scaffolds: Synthesis, biological activity, and X-ray crystal-structure analysis. *Helv. Chim. Acta* **2005**, *88*, 731−750.

(13) Glossop, M. S.; Bazin, R. J.; Dack, K. N.; Fox, D. N. A.; MacDonald, G. A.; Mills, M.; Owen, D. R.; Phillips, C.; Reeves, K. A.; Ringer, T. J.; Strang, R. S.; Watson, C. A. L. Synthesis and evaluation of heteroarylalanine diacids as potent and selective neutral endopeptidase inhibitors. *Bioorg. Med. Chem. Lett.* **2011**, *21*, 3404−3406.